Shell-model influence in the rotational nucleus ^{86}Mo

D. Rudolph,[1,*] C. J. Gross,[1,2] Y. A. Akovali,[1] C. Baktash,[1] J. Döring,[3] F. E. Durham,[4] P.-F. Hua,[5] G. D. Johns,[3] M. Korolija,[5] D. R. LaFosse,[5] I. Y. Lee,[6] A. O. Macchiavelli,[6] W. Rathbun,[6] D. G. Sarantites,[5] D. W. Stracener,[1] S. L. Tabor,[3] A. V. Afanasjev,[7,†] and I. Ragnarsson[7]

[1]*Physics Division, Oak Ridge National Laboratory, Oak Ridge, Tennessee 37831*

[2]*Oak Ridge Institute for Science and Education, Oak Ridge, Tennessee 37831*

[3]*Department of Physics, Florida State University, Tallahassee, Florida 32306*

[4]*Department of Physics, Tulane University, New Orleans, Louisiana 70118*

[5]*Chemistry Department, Washington University, St. Louis, Missouri 63130*

[6]*Nuclear Science Division, Lawrence Berkeley National Laboratory, Berkeley, California 94720*

[7]*Department of Mathematical Physics, Lund Institute of Technology, Box 118, S-22100 Lund, Sweden*

(Received 14 March 1996)

High-spin states in ^{86}Mo were studied by means of the fusion evaporation reaction ^{58}Ni(^{32}S,$2p2n$)^{86}Mo at 135 MeV beam energy. Charged-particle-$\gamma\gamma$ and -$\gamma\gamma\gamma$ coincidences recorded with the early implementation of the GAMMASPHERE array and the MICROBALL charged-particle detection system were used to largely extend the level scheme of the $T_z=1$ nucleus ^{86}Mo to a possible spin of $I=24\hbar$ at 13 MeV excitation energy. The excitation scheme is compared to neighboring nuclei. There is evidence for enhanced shell-model influence in the 4 quasiparticle region ($I=12$–$16\,\hbar$). The observed ($\pi=+,\alpha=0$) sequence at spin $I\geqslant 16\hbar$ appears to be associated with a triaxial collective rotational band. This interpretation is supported by calculations within the configuration-dependent shell-correction approach with the cranked Nilsson potential.
[S0556-2813(96)03607-2]

PACS number(s): 21.10.Re, 21.60.Cs, 23.20.Lv, 27.50.+e

I. INTRODUCTION

The dividing line between well-deformed nuclei with rotational bands and less collective nuclei is rather sharp in the neutron deficient mass region $A\approx 90$ [1]. The nuclei with $N\leqslant 44$ exhibit rotational bands whereas the nuclei with $N\geqslant 47$ are less collective and can be adequately described in terms of the shell model. The $N=46$ isotopes are considered to be transitional nuclei, but are essentially described by the spherical shell model [2]. The shell-model structures are also manifested in the so-called band terminating states in some Sr isotopes [3,4]. In the transition region ($N\approx 45$) quasiparticle (qp) alignment may strongly influence the collectivity of excited states as has been observed in ^{87}Mo [5]. The measured collectivity in the 3 qp band exceeds that of the 1 qp states by a factor of about 6. However, the $B(E2)$ strengths in the $N=46$ isotopes ^{87}Nb and ^{88}Mo decrease by about a factor of 4 after the first quasiparticle alignment [6,7]. With such rapid changes in collectivity nearby, the $N=44$ isotones with $Z>40$ may exhibit rotational structures influenced by single-particle excitations. Therefore, we have undertaken a study of ^{86}Mo. In this nucleus, proton and neutron $g_{9/2}$ orbitals are filled in a similar way and their deformation-driving as well as shell-model effects could act in unison. In addition, residual neutron-proton interactions may play a significant role in the structure of the isospin $T_z=1$ nucleus ^{86}Mo. Isospin was found to be important with respect to band crossing phenomena of nuclei close to $N=Z$ [8].

Recently, the powerful γ-ray detector arrays GAMMASPHERE and EUROGAM allowed the observation of the predicted [9,10] superdeformed (SD) shell gaps for particle number of $Z,N\approx 44$ [4]. Jin *et al.* [11] confirmed the large quadrupole deformation of a SD band in the ^{86}Mo isotone ^{84}Zr ($N=44$, $\beta_2=0.53$) with the residual Doppler shift method. In ^{82}Sr [12], another $N=44$ isotone of ^{86}Mo, two SD bands have been observed.

Little information on excited states in ^{86}Mo was previously reported. Gross *et al.* [13] were able to identify a possible $4^+\rightarrow 2^+\rightarrow 0^+$ cascade for the first time via recoil-γ coincidences. The transition energies (568 and 761 keV) indicate the beginning of a rotational band built upon a moderately deformed ground state in agreement with predictions from Hartree-Fock cranking calculations [13]. Subsequently, Mitarai *et al.* [14] reported two more γ rays (933 and 972 keV) that extend the positive-parity yrast band. The present study aimed at extending the positive-parity yrast sequence beyond the band crossing region, establishing negative-parity states, and possibly identifying superdeformed structures. In the following section, details of the experiment and the new level scheme will be presented. In Sec. III the new results will be compared with the level schemes of neighboring, well-established isotopes and isotones and the high-spin data will be compared with calculations using the Nilsson-Strutinsky cranking model.

II. EXPERIMENT, DATA REDUCTION AND LEVEL SCHEME

The experiment was performed at the 88-inch Cyclotron at the Lawrence Berkeley National Laboratory. The

*Present address: Sektion Physik der Universität München, Am Coulombwall 1, D-85748 Garching, Germany.

†Permanent address: Nuclear Research Center, Latvian Academy of Sciences, LV-2169, Salaspils, Miera str. 31, Latvia.

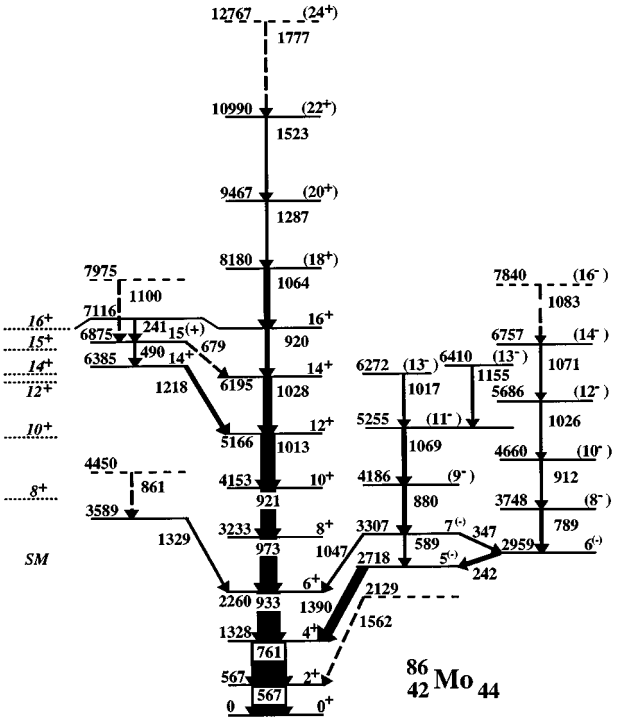

FIG. 1. Proposed partial level scheme of ^{86}Mo. The energy labels are given in keV. The widths of the arrows are proportional to the relative intensities of the γ rays. Shown on the left-hand side are the calculated $I=8-16\hbar$ shell-model states.

^{58}Ni(^{32}S,$2p2n$)^{86}Mo reaction at 135 MeV bombarding energy was used to populate excited states in ^{86}Mo. The target consisted of a 99.7% highly enriched self-supporting ^{58}Ni foil of 210 μg/cm^2 which was rotated 30° relative to the beam direction. The experimental setup consisted of the early implementation of the GAMMASPHERE array [15] comprising 36 Compton-suppressed Ge detectors, and the Washington University MICROBALL [16], which is a 4π charged-particle detector array with 95 CsI(Tl) scintillators. The event trigger required coincidences between three or more Ge detectors. A total of 4.2×10^8 raw events were collected. The events were sorted off-line into E_γ-E_γ matrices subject to the appropriate charged-particle gates. The final $2p$-gated matrix had 4.9×10^8 events, including contaminants of the strong reaction channels ^{84}Zr+$\alpha2p$, ^{87}Nb+$3p$, and ^{86}Zr+$4p$ which leaked through when an α particle or one or more protons were not detected. Successive subtraction of the higher fold charged-particle channels finally led to a ''pure'' $2p\gamma\gamma$ matrix with 4.3×10^7 events. This matrix contained only γ rays originating from ^{88}Mo+$2p$ ($\approx$10%), ^{87}Mo+$2pn$ ($\approx$ 60%), and ^{86}Mo+$2p2n$ ($\approx$ 30%). ^{87}Mo [5] and ^{88}Mo [17] are well known, thus allowing the identification of possible doublet structures of γ rays originating from ^{86}Mo and one of those reaction channels. Coincidence, intensity, and summed energy relations were used to deduce the greatly extended level scheme illustrated in Fig. 1 and summarized in Table I. For example, Fig. 2(b) illustrates the γ-ray spectrum gated with the 567-keV $2^+\rightarrow0^+$ transition, which shows a series of previously unknown lines in addition to the reported ones at 761, 933, and 972 keV (here 973 keV). Similarly, Fig. 2(a) represents the sum of the

TABLE I. The energies of excited states in ^{86}Mo, the transition energies and relative intensities of the γ rays placed in the level scheme, the DCO ratios and the gate used to obtain them, and the spins and parities of the initial and final states of the γ rays.

E_x (keV)	E_γ (keV)	$I_{\rm rel}$ (%)	$R_{\rm DCO}$	Gate [a]	I_i^π ($\hbar$)	I_f^π ($\hbar$)
566.6(4)	566.6(4)	100(3)			2^+	0^+
1327.5(6)	760.9(5)	100(3)	1.01(9)	*A*	4^+	2^+
2129(2)	1562(2)	4(1)				2^+
2260.1(9)	932.6(6)	68(5)	1.05(8)	*B*	6^+	4^+
2717.7(12)	1390(1)	26(3)	0.68(11)	*A*	$5^{(-)}$	4^+
2959.4(13)	241.7(4)	13(3)	0.62(8)	*B*	$6^{(-)}$	$5^{(-)}$
3232.8(11)	972.7(7)	49(5)	0.92(11)	*B*	8^+	6^+
3306.5(8)	347.1(5)	6(1)	0.60(20)	*B*	$7^{(-)}$	$6^{(-)}$
	588.5(6)	10(2)	1.05(29)	*B*	$7^{(-)}$	$5^{(-)}$
	1047(1)	5(2)			$7^{(-)}$	6^+
3589(2)	1329(1)	11(2)				
3748(2)	789(1)	10(2)	1.12(20)	*B*	(8^-)	$6^{(-)}$
4153.4(13)	920.6(7)[b]	45(5)	1.08(11)	*B*	10^+	8^+
4186(1)	879.9(6)	17(2)	1.08(21)	*A*	(9^-)	$7^{(-)}$
4450(2)	861(1)	5(2)				
4660(2)	912(1)	9(2)			(10^-)	(8^-)
5166.4(15)	1013(1)	42(4)	1.10(14)	*A*	12^+	10^+
5255(1)	1069(1)	15(2)			(11^-)	(9^-)
5686(3)	1026(1)	8(1)			(12^-)	(10^-)
6195(2)	1028(1)	28(3)	1.05(10)	*C*	14^+	12^+
6272(2)	1017(1)	9(2)			(13^-)	(11^-)
6385(2)	1218(1)	15(2)	1.10(28)	*C*	14_2^+	12^+
6410(2)	1155(1)	5(2)			(13_2^-)	(11^-)
6757(3)	1071(2)	6(1)			(14^-)	(12^-)
6875(2)	490.3(5)	9(2)	0.48(11)	*C*	$15^{(+)}$	14_2^+
	679(1)	2(1)			$15^{(+)}$	14^+
7116(2)	241(1)	5(1)	0.67(31)	*D*	16^+	$15^{(+)}$
	920(1)[b]	17(3)	1.08(11)	*B*	16^+	14^+
7840(4)	1083(2)	4(1)			(16^-)	(14^-)
7975(2)	1100(1)	6(2)				$15^{(+)}$
8180(2)	1064(1)	21(3)			(18^+)	16^+
9467(3)	1287(1)	10(2)			(20^+)	(18^+)
10990(3)	1523(2)	6(2)			(22^+)	(20^+)
12767(4)	1777(2)	2(1)			(24^+)	(22^+)

[a] *A*, 567 keV; *B*, 567+761 keV; *C*, 567+761+933 keV; *D*, 933 +973+921 keV.

[b] Doublet structure.

γ-ray spectra gated with the 1390- and 242-keV transitions. The 1390-keV transition carries most of the γ-ray flux from the negative- to positive-parity states. The 242-keV transition is the connection between the two signature partners of the negative parity. In order to make use of triple coincidences, a $2p$-gated $\gamma\gamma\gamma$ cube and a second $2p$-gated $\gamma\gamma$ matrix were sorted. For the latter, the additional condition that the double event be in coincidence with a third γ ray at 242, 347, 567, 761, 921, 933, 973, or 1390 keV was imposed. Figure 2(c) is the sum of the γ-ray spectra gated with the 933-, 973-, and 921-keV transition in this ''triples'' matrix illustrating the positive-parity band. As will be seen later on, the location of the two low energy transitions at 490 and

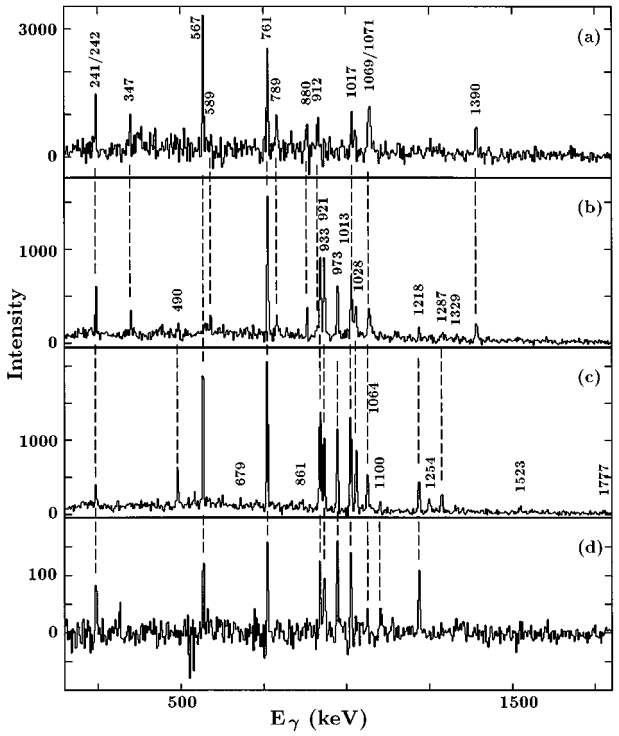

FIG. 2. Coincidence spectra of ^{86}Mo: (a) sum of the spectra in coincidence with the 242 and 1390 keV transitions in the ''pure'' $2p\gamma\gamma$ matrix; (b) spectrum gated with the 567 keV transition in the ''pure'' $2p\gamma\gamma$ matrix; (c) sum of the spectra in coincidence with the 921-, 933-, and 973-keV transitions in the ''triples'' $2p\gamma\gamma$ matrix; and (d) spectrum gated with the 490-keV transition in the ''triples'' $2p\gamma\gamma$ matrix. The energy labels are given in keV.

241 keV (doublet with the 242-keV transition in the negative parity) is important in the understanding of the structure of ^{86}Mo. Figure 2(d) shows the spectrum gated with the 490-keV transition in the ''triples'' matrix. The transitions at 567, 761, 921, 933, 973, 1013, and 1218 keV all have about the same intensity, whereas the 241-, 1064-, and 1100-keV transitions are present but with weaker intensities. Thus the position of the 490-keV transition is unambigously determined.

The geometry of the GAMMASPHERE also allowed the assignments of spins from the angular correlations of the γ rays. For this purpose, a matrix was constructed in which γ events recorded at 90° were sorted against those recorded at 17°, 31°, 37°, 143°, 149°, or 163° in coincidence with two protons detected in MICROBALL. The 30 Ge detectors at the latter six angles were combined to provide a maximum of statistics. The cosines of the angles at 17° (163°), 31° (149°), and 37° (143°) average to the cosine of an angle at approximately 30° (the angular distribution of γ rays following heavy ion fusion evaporation reactions is symmetric with respect to 90°). Pairs of gated spectra may be used to obtain directional correlations of oriented states (DCO ratios), defined as

$$R_{\mathrm{DCO}}(\gamma_1,\gamma_2)=\frac{I(\gamma_1 \text{ at } 30°;\ \text{gated with}\ \gamma_2 \text{ at } 90°)}{I(\gamma_1 \text{ at } 90°;\ \text{gated with}\ \gamma_2 \text{ at } 30°)}, \quad (1)$$

when γ_2 is a stretched $E2$ transition. The DCO ratios were not corrected for detection efficiency because the relative efficiency of the detectors at ''30°'' and 90° were found to be equal within the 3% accuracy of the efficiency calibration. The DCO ratios obtained are given in Table I together with the corresponding gates. In most cases gates were summed up in order to improve statistics. This procedure does not significantly affect the results as shown in a work by Kabadiyski *et al.* [18]. The expected DCO ratios are $R_{\mathrm{DCO}}=1.0$ for a stretched $E2$ transition and $R_{\mathrm{DCO}}\approx 0.5$ for a stretched dipole transition. Depending on the multipole mixing ratio $\delta(E2/M1)$ the DCO-ratio may differ from $R_{\mathrm{DCO}}=0.5$.

The level scheme in Fig. 1 is dominated by the positive-parity yrast structure. It consists of 12 consecutive stretched $E2$ transitions. Up to the 7116 keV 16^+ state, the spin assignments are based on the DCO ratios in Table I. Thereafter, the magnitude and the regular increase of the γ-ray energies strongly suggests stretched $E2$ character for these transitions. According to their DCO ratios, the 490-[$R_{\mathrm{DCO}}=0.48(11)$] and 241-keV [$R_{\mathrm{DCO}}=0.67(31)$] transitions have stretched dipole character or are consistent with stretched dipole character, respectively. This allows, in principle, positive or negative parity for the 6875-keV level. However, negative parity is very unlikely as the $E1$ strength of the 241-keV transition would be orders of magnitude higher than usual with respect to the parallel 920-keV $E2$ transition. The positive-parity sequence extends to a tentative 24^+ state at an excitation energy of 12767 keV — the highest excitation energy and spin observed so far for a $T_z=1$ nucleus. The doublet structure of the 921-keV $10^+\rightarrow 8^+$ and the 920-keV $16^+\rightarrow 14^+$ transition was deduced from (a) a self-coincidence in both the ''pure'' $2p$-gated matrix and the ''triples'' matrix, (b) the intensity relationships in spectra gated with the 1028- and 1218-keV $14^+\rightarrow 12^+$ transitions, and (c) the coincidences between the 1028-keV $14^+\rightarrow 12^+$ and the 1064-keV $18^+\rightarrow 16^+$ transition, which cannot be explained by the weak $16^+\rightarrow 15^{(+)}\rightarrow 14^+$ bypass. This coincidence also provides a lower intensity limit for the 920-keV transition. The doublet complicated the determination of the level order between the 2260-keV 6^+ and the 5166-keV 12^+ states, because the 973-, 921-, and 1013-keV transitions are almost equally strong. However, the inspection of relative intensities in a series of gated spectra with transitions below the 6195-keV 14^+ state provided enough evidence for the order presented in Fig. 1. The relative intensities of the three transitions in Table I are consistent.

A specific feature in the ^{86}Mo decay scheme is the $\Delta I=1$, $16^+\rightarrow 15^{(+)}\rightarrow 14_2^+$ cascade which carries about 25% of the γ-ray flux out of the 7116-keV 16^+ state. In the case of a rotating even-even nucleus in the $A\approx 80$–90 region the decay down the positive-parity yrast cascade consists exclusively of stretched $E2$ transitions, e.g., in ^{82}Zr [19] or ^{84}Zr [11]. However, intense $16^+\rightarrow 15^{(+)}\rightarrow 14^+$ sequences have been observed in the heavier ($N\geqslant 46$) even-even Zr, Mo, and Ru isotopes [20,17,21]. The 861- and 1329-keV transitions feeding the 2260-keV 6^+ state might depopulate the yrare 10^+ and 8^+ states. However, the transitions are too weak to deduce spin assignments from the present experiment. The transition at 1254 keV, which can be clearly seen in Fig. 2(c), most probably also belongs to ^{86}Mo but could not be placed in the level scheme due to lack of statistics.

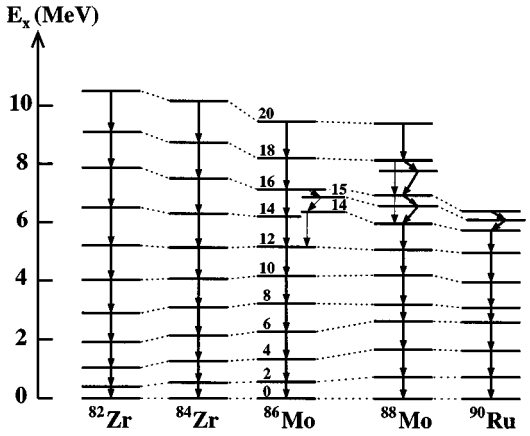

FIG. 3. Comparison of the positive-parity yrast levels of ^{82}Zr ($T_z=1$, $N=42$) [19], ^{84}Zr ($T_z=2$, $N=44$) [1,11], ^{86}Mo ($T_z=1$, $N=44$), ^{88}Mo ($T_z=2$, $N=46$) [17], and ^{90}Ru ($T_z=1$, $N=46$) [21].

The DCO ratio of the 1390-keV transition is consistent with a $\Delta I=1$ transition with a vanishing mixing ratio δ. Thus it is most likely the parity changing $5^-\rightarrow 4^+$ transition. The tentative assignment is based on the analogy with the neighboring even-even nuclei (In most cases, the main flux from the negative- to positive-parity states is carried by a $5^-\rightarrow 4^+$ transition of about 1.0–1.5 MeV.) The spin assignments of the 2959-keV $6^{(-)}$ and 3307-keV $7^{(-)}$ states arise from the DCO ratios of the 242- and 347-keV and the observed parallel 589-keV transition. Beyond, the magnitude of the γ-ray energies and the excitation pattern again favor $E2$ character. The placement of the 912-keV transition (close to the 915-keV $4^+\rightarrow 2^+$ transition in the strongest reaction channel ^{86}Zr) and the 1069/1071-keV doublet was possible only by using the $2p$-gated $\gamma\gamma\gamma$ cube. Superdeformed structures were not observed for ^{86}Mo in the present experiment.

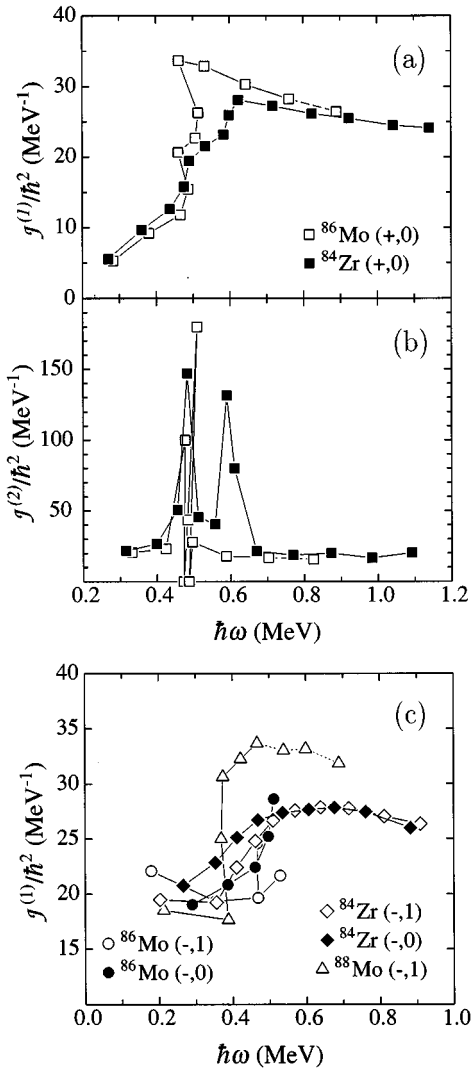

FIG. 4. Kinematic ($\mathcal{J}^{(1)}$) and dynamic ($\mathcal{J}^{(2)}$) moments of inertia for the positive-parity yrast structures of ^{84}Zr [1,11] and ^{86}Mo.

III. DISCUSSION

A. Systematics and shell-model influence

In Fig. 3, the positive-parity yrast sequence of ^{86}Mo is compared to those in the even-even neighbors ^{82}Zr [19], ^{84}Zr [1,11], ^{88}Mo [17], and ^{90}Ru [21] up to spin $I^\pi=20^+$. The two lighter Zr isotopes were interpreted in terms of rotational bands, whereas the two $N=46$ isotones reveal typical features of transitional nuclei. The states up to the first alignment of a broken $g_{9/2}$ proton or neutron pair, i.e., spin $I=8$, are consistent with the rotation of a weakly deformed ground state ($\beta_2\approx 0.1$–0.2). Thereafter, the structure of these isotopes is dominated by the shell-model states, although enhanced $B(E2)$ strengths have been observed [2]. The similarity of the ^{86}Mo yrast sequence to its isotone ^{84}Zr is striking (see also Fig. 4). This suggests a collective approach for the interpretation of ^{86}Mo. However, the correspondence of the $16^+\rightarrow 15^{(+)}\rightarrow 14_2^+$ $\Delta I=1$ cascade to the $N=46$ nuclei points to an enhanced shell-model influence in that part of the level scheme.

To study this influence in some detail, a shell-model calculation based on a set of empirical two-body matrix-elements [22] was performed. Using ^{88}Sr as the core, the configuration space consisted of only the $2p_{1/2}$ and $1g_{9/2}$ orbitals for protons and neutrons. Effective charges ($\tilde{e}_\pi=1.72$ and $\tilde{e}_\nu=1.44$) and effective g factors ($g_l(\pi)=0.97$, $g_s(\pi)=4.70$, $g_l(\nu)=0.13$, and $g_s(\nu)=-3.24$) were used to describe the transition rates. This parametrization (GF-1 as labeled and presented in detail in Ref. [2]) was found to describe $A\approx 90$ nuclei with $N\geqslant 46$ very well. The main result is that due to the strong interaction between neutrons and protons moving in nearly identical $g_{9/2}$ orbits, the 14^+, 15^+, and 16^+ states lie comparatively low in energy. The latter are predicted to contain mainly the seniority $v=4$ partitions $[\pi(g_{9/2})_8^2\otimes\nu(g_{9/2})_8^{-2}]_{15}$ (48%) and $[\pi(g_{9/2})_8^2\otimes\nu(g_{9/2})_8^{-2}]_{16}$ (78%) with completely aligned neutron and proton subconfigurations in either case. This allows for a strong $M1$ transition between these states. The predicted γ-ray energies are 389 keV ($16^+\rightarrow 15^+$) and 452 keV ($15^+\rightarrow 14^+$), reasonably close to the observed 241 and 490 keV. The calculated positive-parity yrast levels are shown on the left-hand side in Fig. 1 (SM). They are normalized to the energy of the 7116-keV 16^+ state.

The following additional remarks concerning the possible interplay between collective and shell-model states in the 4 qp region of ^{86}Mo may be made. The predicted (but not

observed) 12^+ shell-model state lies only 164 keV below the predicted 14^+ shell-model state. This small transition energy and the difference in the configurations of the initial and final states would lead to a predicted isomeric 14^+ shell-model state: $\tau_{\text{theo}}(14^+)=80$ ns. The decay of the 14_2^+ state (if associated with the 14^+ shell-model state) into the 12^+ collective yrast state would then be competitive, as possibly observed with the 1218 keV $14_2^+ \rightarrow 12^+$ transition. Perhaps the best observable regarding shell-model influence in this part of the level scheme is the lifetime of the 6385 keV 14_2^+ state. If shell-model admixtures to its wave function were present, its lifetime should amount to at least several picoseconds (correponding to a stopped peak in a Doppler-shift attenuation lifetime experiment) as compared to subpicosecond lifetimes of states located at similar excitation energies within rotational bands of neighboring nuclei (corresponding to Doppler-shifted and -broadened line shapes). It is interesting to note that in the latest work on ^{84}Zr [11] a $17^+ \rightarrow 15^+ \rightarrow 14_2^+ \rightarrow 12^+$ cascade was observed with similar transition energies as in ^{86}Mo. However, the corresponding $16^+ \rightarrow 15^+$ transition was not reported. The energy difference between the calculated 16^+ and 8^+ states amounts to 3.1 MeV, as compared to 3.5 MeV between the experimental 16^+ state and the 3589 keV state. Hence, the observed levels at 3589 and 4450 keV might be associated with shell-model states.

The shell-model calculation yields a branching ratio $b=b_1(16^+ \rightarrow 15^+)/b_2(16^+ \rightarrow 14^+)=7.3$ and, as expected, overestimates the $\Delta I=1$ branch $(b=[\lambda(M1; 16^+ \rightarrow 15^+)+\lambda(E2;16^+ \rightarrow 15^+)]/[\lambda(E2; 16^+ \rightarrow 14^+) +\lambda_{\text{coll}}(E2;16^+ \rightarrow 14^+)]$ with λ representing the partial decay widths). To reproduce the measured branching ratio $b_{\text{expt}}=0.29(^{14}_{9})$, an additional collective $E2$ strength of $B(E2;16^+ \rightarrow 14^+)_{\text{coll}} \approx 1700$ e^2 fm^4 would be necessary. This suggests a mixed character for the 7116-keV 16^+ state. Assuming an axially deformed prolate rotor, the additional collective strength corresponds to a deformation of $\varepsilon_2 \approx 0.24$ (ε_2 is approximately equal to $0.94\beta_2$). This is in good agreement with the total Routhian surface (TRS) map deduced in Ref. [13] using a Hartree-Fock-Bogolyubov cranking calculation with a nonaxial Woods-Saxon potential. The authors reported a spherical ground state and a triaxial minimum in the ε_2-γ plane at $(0.25,-30°)$ at a rotational frequency of $\hbar\omega \approx 0.3$ MeV which is only 160 keV above the spherical minimum. A cranking calculation using the Strutinsky method and the modified harmonic oscillator potential provides similar results [23]: a minimum in the TRS map at $(\varepsilon_2=0.25, \gamma=-32°)$ for the ground state configuration. Kirchuk *et al.* [24] calculated the ground state deformation to $\varepsilon_2 \approx 0.1$ with an axially symmetric Hartree-Fock-Bogolyubov calculation. The calculations within the cranked Nilsson-Strutinsky model (see Sec. III B) indicate the deformation $\varepsilon_2=0.22, \gamma=-49°$ for the yrast $I=16^+$ state.

Figures 4(a) and 4(b) show the kinematic and dynamic moments of inertia for the positive-parity yrast structures in ^{86}Mo and ^{84}Zr [1,11]. In Fig. 5 the alignment i with respect to a reference rotor with the Harris parametrization [25] $(\mathcal{J}_0, \mathcal{J}_1, i_0)=(20\hbar/\text{MeV}, 0, -4\hbar)$ is illustrated for ^{86}Mo and ^{84}Zr and their odd-Z $N=44$ isotones ^{85}Nb [26] and ^{87}Tc [27]. The Harris parameters are based on the nearly constant

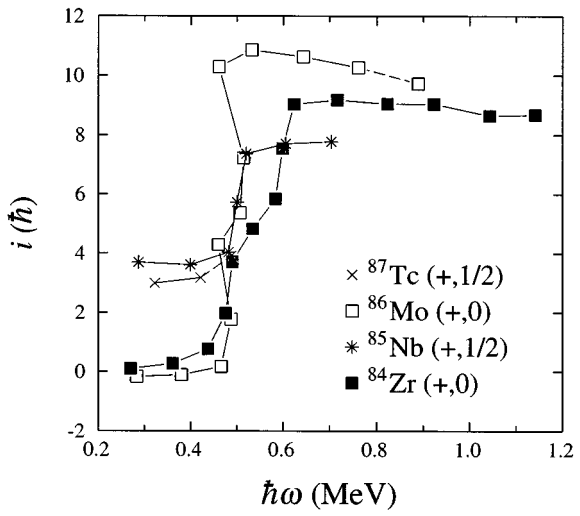

FIG. 5. Quasiparticle alignment i of the positive-parity yrast structures of the $N=44$ isotones ^{84}Zr [1,11], ^{85}Nb [26], ^{86}Mo, and ^{87}Tc [27].

and equal moments of inertia of ^{84}Zr after the two band crossings [see Fig. 4(b)]. Both ^{86}Mo and ^{84}Zr show their first steep back- and upbend at a rotational frequency of $\hbar\omega=0.48$ MeV. By means of a transient field g-factor measurement in ^{84}Zr, Mountford *et al.* [28] demonstrated that the aligning particles of this crossing are $g_{9/2}$ protons. The identity in the crossing frequency and the amount of the alignment strongly suggest the same nature for the first crossing in ^{86}Mo. This interpretation is also in agreement with an investigation of yrast and yrare 8^+ states in even-even nuclei in the $A=80$–90 region. In the more collective region with $N \leqslant 44$ the predicted and/or observed g factors of the yrast 8^+ states are positive, indicating $g_{9/2}$ proton alignment taking place first. In contrast, the more shell-model-like nuclei with $N \geqslant 46$ provide negative g factors for the yrast 8^+ states [29].

The second band crossing in ^{86}Mo at $\hbar\omega=0.51$ MeV immediately follows the first one. In ^{84}Zr, it is delayed to $\hbar\omega=0.60$ MeV. For both nuclei, the total alignment amounts to about $10\hbar$, consistent with the breaking of two pairs of $g_{9/2}$ nucleons. After the crossings, both isotopes assume similar dynamic and kinematic moments of inertia. The odd-A isotone ^{85}Nb reveals only one upbend at exactly the same frequency as the second crossing in ^{86}Mo. The amount of alignment is about half of that of the even-even nuclei. In ^{85}Nb, the first $g_{9/2}$ proton alignment is Pauli-blocked due to the unpaired proton. Hence, Gross *et al.* [26] suggested the upbend to reflect a neutron $g_{9/2}$ quasiparticle alignment, consistent with the interpretation of the ^{86}Mo band.

On the negative-parity side two 13^- states are observed, one of which might represent a seniority $v=4$ completely aligned shell-model state, with either one proton or one neutron occupying the $p_{1/2}$ shell. However, the existence of both signatures with almost no signature splitting strongly suggests mainly rotational excitation for the negative parities as well. Although the transition energies of the negative-parity states in the neighboring transitional and shell-model-like nuclei (e.g., ^{88}Mo, Ref. [17]) are also around 1 MeV and nearly equally spaced, the odd-spin states are favored in ex-

citation energy. Figure 4(c) illustrates the kinematic moments of inertia for the negative-parity structures in ^{86}Mo and compares them to the negative-parity rotational bands in the $N=44$ isotone ^{84}Zr [1,11] and the shell-model-like odd-spin sequence in the $Z=42$ isotope ^{88}Mo [17]. The final three data points of ^{88}Mo correspond to the 19^-, 21^-, and 23^- states. Since the $19^-\rightarrow 17^-$ $E2$ transition was not observed and the $21^-\rightarrow 19^-$ $E2$ transition was found to be much weaker than the accompanying two $\Delta I=1$ transitions [17], the connections in Fig. 4(c) are dotted. Those $\Delta I=1$ transitions on top of the sequence in conjunction with an abnormally large sudden increase and saturation value of $\mathcal{J}^{(1)}$ [see Fig. 4(c) disagrees with the interpretation of a rotational band. In fact, transition energies [17] and probabilities [2] are well reproduced by shell-model calculations. On the other hand, the bands in ^{84}Zr show a gradual alignment of some $6\hbar$ at a rotational frequency of $\hbar\omega\approx 0.45$ MeV. This is consistent with the alignment of a $g_{9/2}$ pair of nucleons and the moments of inertia saturate at values similar to the positive-parity yrast band in that nucleus [see Fig. 4(a)]. The behavior of the bands in ^{86}Mo lies in between these two examples. The beginning of an upbend around $\hbar\omega=0.5$ MeV can be seen, but the lack of experimental data at high spins prohibits a definitive conclusion of whether the bands have mainly shell-model character (like ^{88}Mo) or represent rotational bands (like ^{84}Zr).

B. Cranked Nilsson-Strutinsky calculations

The nuclei in the neutron-deficient $A\approx 80$–90 mass region undergo drastic changes in deformation as function of neutron and proton number [30]. For example, the nuclei with $N\approx 44$ are expected to be γ soft [13,23]. This suggests the existence of triaxial collective bands in the yrast or near-yrast region of ^{86}Mo at high spin. At large enough spin, this picture can become even richer by termination of different bands.

In the present work, the configuration-dependent shell-correction approach with the cranked Nilsson potential [31] is employed for detailed investigation of the high-spin states in ^{86}Mo. This approach allows us to consider the collective and terminating bands on the same footing. Pairing correlations are neglected in the present calculations. Because the standard set of Nilsson potential parameters [31] does not reproduce correctly the relative position of $g_{9/2}$, $f_{5/2}$, and $p_{1/2}$ spherical states in this mass region [32], we use the parameter set adjusted for ^{86}Zr [33]. Since pairing correlations are neglected, our calculations can be considered as realistic at high spin, say $I\geqslant 15\hbar$. This means that when comparing experiment and theory, one should not use absolute energies relative to the ground state. Instead, the relevant values are the energies measured relative to some high-spin state. One should also note that, with approximations which are negligible at small deformation, the cranked Nilsson Hamiltonian is diagonalized in the present calculations. After the diagonalization, however, it is generally possible to characterize each orbital as being dominated by one j shell and this j shell (e.g., $g_{9/2}$, $f_{5/2}$, or $p_{1/2}$) is then used to get an instructive label for different orbitals.

The results of calculations are compared with experimental data in Fig. 6(a). The configurations are summarized in Table II and will be refered to with bold arabic numbers in the text. The shape trajectories in the ε_2,γ plane for configurations **1–6** are shown in Fig. 6(b). All calculated bands terminate in noncollective oblate shapes ($\gamma=60°$ or $\gamma=-120°$). In configuration **1** with a closed $^{80}_{40}\mathrm{Zr}_{40}$ core, $\pi(g_{9/2})^2_8\otimes\nu(g_{9/2})^4_{12}$, the maximum available spin is $I_{\max}=20\hbar$. Higher spin states with ($\pi=+,\alpha=0$) can be obtained, for example, by excitation of two protons from the

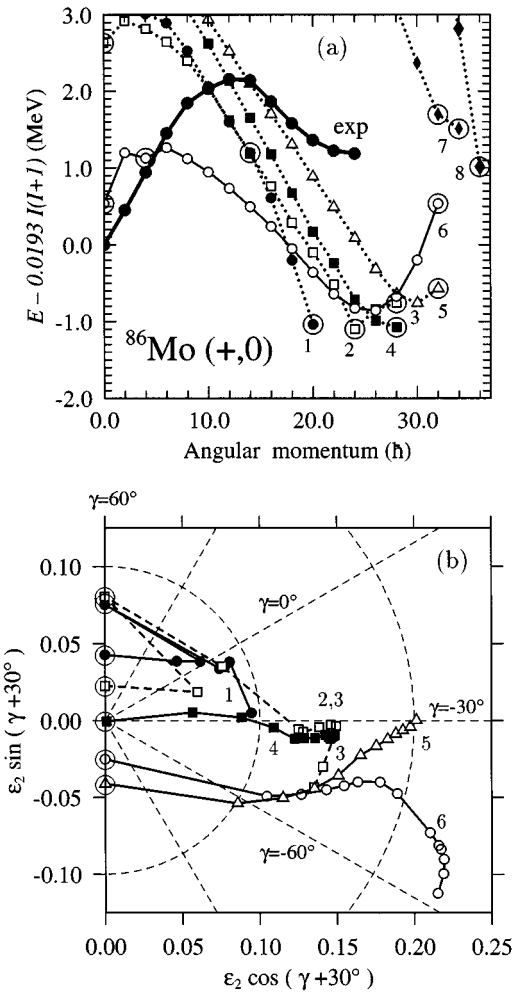

FIG. 6. (a) Calculated level energies for various configurations of positive parity and signature $\alpha=0$ in the yrast region of ^{86}Mo. The energies are given relative to a smooth liquid-drop expression $(\hbar^2/2\mathcal{J}_{\mathrm{rig}})I(I+1)$, where the moment of inertia parameter is $(\hbar^2/2\mathcal{J}_{\mathrm{rig}})=0.0193$ MeV. Noncollective states ($\gamma=60°$ or $\gamma=-120°$) are encircled. The observed ($\pi=+,\alpha=0$) sequence is shown by large solid symbols and a solid line. Configuration **6** is shown by a solid line and open circles. Other calculated configurations (**1**, **2-3**, **4**, and **5**) are shown by dotted lines and the solid circles, open squares, solid squares, and open triangles, respectively. Configurations **2-3** are shown by one line because low-j $p_{1/2}$ and $f_{5/2}$ orbitals are mixed strongly. This line corresponds to the lowest in energy solution within the group of configurations $\pi[(g_{9/2})^4_{12}(N=3)^{-2}_X]_{12+X}\otimes\nu(g_{9/2})^4_{12}$. (b) Shape trajectories in the ε_2,γ plane for configurations **1–6**. The same symbols as in (a) are used to indicate the calculated configurations. The deformation points are given in steps of $2\hbar$. The initial spin is $6\hbar$ for all configurations except for configuration **5** whose shape trajectory is shown from $I=10\hbar$.

TABLE II. Suggested configurations at the band termination of the near-yrast structures in ^{86}Mo with parity and signature quantum number (+,0).

1	$\pi(g_{9/2})^2_8 \otimes \nu(g_{9/2})^4_{12}$
2	$\pi[(g_{9/2})^4_{12}(p_{1/2})^{-2}_0]_{12} \otimes \nu(g_{9/2})^4_{12}$
3	$\pi[(g_{9/2})^4_{12}(f_{5/2})^{-2}_4]_{16} \otimes \nu(g_{9/2})^4_{12}$
4	$\pi[(g_{9/2})^3_{10.5}(f_{5/2})^{-1}_{2.5}]_{13} \otimes \nu[(g_{9/2})^5_{12.5}(f_{5/2})^{-1}_{2.5}]_{15}$
5	$\pi[(g_{9/2})^5_{12.5}(f_{5/2}p_{1/2})^{-3}_{4.5}]_{17} \otimes \nu[(g_{9/2})^5_{12.5}(f_{5/2})^{-1}_{2.5}]_{15}$
6	$\pi[(g_{9/2})^4_{12}(f_{5/2})^{-2}_4]_{16} \otimes \nu[(g_{9/2})^6_{12}(f_{5/2})^{-2}_4]_{16}$
7	$\pi[(g_{9/2})^4_{12}(f_{5/2}p_{1/2})^{-3}_{4.5}(h_{11/2})^1_{5.5}]_{22} \otimes \nu(g_{9/2})^4_{12}$
8	$\pi[(g_{9/2})^3_{10.5}(p_{1/2})^{-2}_0(h_{11/2})^1_{5.5}]_{16} \otimes$ $\nu[(g_{9/2})^4_{12}(p_{1/2})^{-2}_0(g_{7/2}d_{5/2})^1_{2.5}(h_{11/2})^1_{5.5}]_{20}$

$N=3$ shell into the $g_{9/2}$ orbitals. The maximum spin for configurations **2** and **3** of positive parity and signature $\alpha=0$ which can be obtained in this way is either $I_{\max}=24\hbar$ $(\pi[(g_{9/2})^4_{12}(p_{1/2})^{-2}_0]_{12} \otimes \nu(g_{9/2})^4_{12})$, $I_{\max}=26\hbar$ $(\pi[(g_{9/2})^4_{12}(p_{1/2})^{-1}_{-0.5}(f_{5/2})^{-1}_{2.5}]_{14} \otimes \nu(g_{9/2})^4_{12})$, or $I_{\max}=28\hbar$ $(\pi[(g_{9/2})^4_{12}(f_{5/2})^{-2}_4]_{16} \otimes \nu(g_{9/2})^4_{12})$ depending on the distribution of proton holes in the Nilsson orbitals dominated by $p_{1/2}$ and $f_{5/2}$ components, respectively. An alternative possibility involves the excitation of one proton and one neutron (configuration **4**) across the spherical $Z=40$ and $N=40$ shell gaps.

If, in addition to the two protons, two neutrons are also excited across the spherical shell gap at particle number 40, the energy will, of course, become higher for spherical shape and not much spin is gained because the $\nu g_{9/2}$ subshell is almost half-filled. The configuration **6** which is formed $(\pi[(g_{9/2})^4_{12}(f_{5/2})^{-2}_4]_{16} \otimes \nu[(g_{9/2})^6_{12}(f_{5/2})^{-2}_4]_{16})$ is however still of great interest because it can gain a lot of energy by acquiring a triaxially deformed shape. The calculations suggest that the collective band formed in this way becomes energetically competitive in a large spin range, and it can be considered as the most probable candidate for the observed $(\pi=+,\alpha=0)$ sequence.

In the calculations, configuration **1**, which is only slightly collective and terminates at $I=20\hbar$, is lowest for spins $I=18,20\hbar$. However, this configuration cannot be assigned to the observed $(\pi=+,\alpha=0)$ sequence which shows a smooth $\mathcal{J}^{(2)}$ for spins $I=16-24\hbar$. The small collectivity of configuration **1** [see Fig. 6(b)] is one possible reason why it was not observed. Another possibility is that configuration **2** should be associated with the observed $(\pi=+,\alpha=0)$ yrast sequence. It is calculated only $\approx 300-400$ keV above configuration **6** at $I=16\hbar$ and it is lowest at $I=24\hbar$. The highest spin $I=24\hbar$ observed in the $(\pi=+,\alpha=0)$ yrast sequence of ^{86}Mo is equal to the terminating spin of this configuration. It is more collective than configuration **1** [see Fig. 6(b)] and less collective than configuration **6**. Configuration **2** reproduces qualitatively the drop of experimental energies relative to a rigid rotor reference. However, the downslope with increasing spin of the $(E-E_{\mathrm{RLD}})$ curve is overestimated in the calculations.

Configuration **6** has the largest collectivity among the configurations calculated in the yrast and near-yrast region at $I \geqslant 14\hbar$ [see Figs. 6(a) and 6(b)]. Moreover, the relative energy values shown by the slope of the experimental $(E-E_{\mathrm{RLD}})$ curve in Fig. 6(a) is reproduced reasonably well above this spin. The kinematic $(\mathcal{J}^{(1)})$ and dynamic $(\mathcal{J}^{(2)})$ moments of inertia of the observed sequence are rather smooth functions of the rotational frequency at $\hbar\omega \geqslant 0.5$ MeV (see Fig. 4) which indicates that there is no change of the configuration along the yrast $(\pi=+,\alpha=0)$ sequence at spins above $I=16\hbar$. Furthermore, the dynamic moment of inertia $\mathcal{J}^{(2)}$ of the observed sequence ($\mathcal{J}^{(2)} \approx 17\hbar^2$/MeV at $\hbar\omega \geqslant 0.6$ MeV) is approximately one-half of the kinematic moment of inertia ($\mathcal{J}^{(1)} \approx 30\hbar^2$/MeV), which indicates a large single-particle contribution typical for this kind of terminating bands (see for example Ref. [34]). The calculated values of $\mathcal{J}^{(2)}_{\mathrm{theo}}$ and $\mathcal{J}^{(1)}_{\mathrm{theo}}$ for configuration **6** are close to the experimental ones at $\hbar\omega \geqslant 0.6$ MeV. In the calculations, this configuration shows rather smooth deformation changes through the (ε_2,γ) plane with increasing spin [see Fig. 6(b)]. For example, the calculated equilibrium deformation is $\varepsilon_2=0.24$, $\gamma=-55°$ at $I=6\hbar$ and $\varepsilon_2=0.22, \gamma=-49°$ at $I=16\hbar$. Finally, this configuration terminates in an unfavored way at spin $I=32\hbar$ and deformation $\varepsilon_2=0.025, \gamma=-120°$ (noncollective rotation around the prolate symmetry axis). However, configuration **2** cannot be fully ruled out from consideration because it is not known to what extent the present parametrization of Nilsson potential is optimized for the mass region under study. If the charge quadrupole moments were measured, it should help to distinguish between these two possibilities.

All of the above-mentioned features which exist both in experiment and in the calculations for configuration **6** are similar to the ones typical for unfavored termination of the rotational bands in the nuclei neighboring to ^{109}Sb [34,35]. In these bands, the high energy cost for building the last few spin units before termination is mainly connected with proton holes in the $g_{9/2}$ orbitals. In comparison with these bands, which are obtained by excitation of protons across the spherical $Z=50$ shell gap, configuration **6** of ^{86}Mo is obtained by excitation of two neutrons and two protons across the spherical $Z=40$ and $N=40$ shell gaps, where the proton and neutron holes in the $f_{5/2}$ subshell play a similar role as the proton $g_{9/2}$ holes in the terminating bands of the $A \approx 110$ mass region.

All yrast or near-yrast states up to spin $I=32\hbar$ are formed by proton and neutron excitations across the spherical $Z=40$ and $N=40$ shell gaps [see Fig. 6(a)]. Higher spin states can be obtained by excitation of particles into the $h_{11/2}$ (or $g_{7/2}$, $d_{5/2}$) subshell across the spherical $Z=50$ and $N=50$ shell gaps [see configurations **7** and **8** in Fig. 6(a)]. The energy cost per spin unit above $I=32\hbar$ is however quite high. This result is consistent with conclusions of Ref. [32]. In comparison with the $N \approx Z \approx 45$ nuclei studied in Ref. [32], the energy cost per spin unit increases significantly at a spin value which is 12 units larger than the maximum spin $(I=20\hbar)$ which can be achieved in the valence space of ^{86}Mo. This is because only two valence protons reside in the $g_{9/2}$ subshell in the valence configuration for $Z=42$. For example, the excitation of one proton from $f_{5/2}$ to $g_{9/2}$ increases the available spin by 5 spin units in ^{86}Mo, while a similar excitation for a $Z=45$ nucleus gives only two additional spin units. With increasing proton number, such an excitation will give a smaller or even negative contribution to the maximum spin, because the $g_{9/2}$ subshell will be more than half-filled.

IV. SUMMARY

The present charged-particle-$\gamma\gamma$ and -$\gamma\gamma\gamma$ coincidence experiment has extended the four previously known levels in ^{86}Mo by some 20 new levels up to 13 MeV excitation energy and probable spin $I^{\pi}=24^{+}$. The combination of a powerful γ-detector array such as GAMMASPHERE and a selective device such as MICROBALL to separate the various reaction channels has demonstrated the potential for detailed spectroscopy of weakly populated nuclei close to $N=Z$. ^{86}Mo reveals itself as a rotational nucleus. The kinematic and dynamic moments of inertia and the aligment pattern of the positive-parity yrast band are very similar to those of its deformed $N=44$ isotones ^{84}Zr and ^{85}Nb rather than to the transitional nucleus ^{88}Mo. The rotational character of a moderately deformed, triaxial ($\varepsilon_2\approx 0.20$–$0.25$, $\gamma\approx -30°$–$50°$) shape of the positive-parity yrast band of ^{86}Mo is also suggested by cranked shell-model calculations for low spin (Refs. [13,23]) as well as high-spin states (present work). At high spins the experimental data is reproduced best with a $\pi[(g_{9/2})^4_{12}(f_{5/2})^{-2}_4]_{16}\otimes\nu[(g_{9/2})^6_{12}(f_{5/2})^{-2}_4]_{16}$ configuration which terminates in an unfavored way at spin $I=32\hbar$, eight units of spin higher than observed. However, a $\Delta I=1$ $16^{+}\rightarrow 15^{+}\rightarrow 14^{+}_2$ cascade was observed which does not fit into the picture of a purely rotational nucleus. Simple shell-model calculations can account for that phenomenon but, of course, cannot reproduce the regularity of the rotational pattern throughout the yrast cascade. Therefore we conclude that some shell-model seniority $v=4$ admixtures might contribute to the wave functions of the 14^{+}_2, 15^{+}, and 16^{+} states but that the structure of ^{86}Mo is basically of rotational nature. Clearly, lifetime measurements are necessary to test this interpretation.

ACKNOWLEDGMENTS

Oak Ridge National Laboratory is managed by Lockheed Martin Energy Research Corp. for the U.S. Department of Energy under Contract No. DE-AC05-96OR22464. This research was supported by an appointment to the Oak Ridge National Laboratory Postdoctoral Research Associates Program administered jointly by the Oak Ridge Institute for Science and Education and Oak Ridge National Laboratory. This work was also supported in part by the U.S. Department of Energy under Contract Nos. DE-AC05-76OR00033 (ORISE), DE-AC03-76SF00098 (LBNL), and Grant No. DE-FG05-88ER40406 (WU) and by the National Science Foundation under Grant No. PHY-9210082 (FSU) and Swedish Natural Science Research Council. A.V.A. and I.R. are grateful for financial support from the Crafoord Foundation and the Royal Swedish Academy of Sciences.

[1] A. A. Chishti *et al.*, Phys. Rev. C **48**, 2607 (1993).
[2] D. Rudolph, K. P. Lieb, and H. Grawe, Nucl. Phys. **A597**, 298 (1996).
[3] D. M. Cullen *et al.* (unpublished).
[4] C. Baktash, D. M. Cullen, J. D. Garrett, C. J. Gross, N. R. Johnson, W. Nazarewicz, D. G. Sarantites, J. Simpson, and T. R. Werner, Phys. Rev. Lett. **74**, 1946 (1995).
[5] Ch. Winter *et al.*, Phys. Lett. B **258**, 289 (1991); Nucl. Phys. **A535**, 137 (1991).
[6] A. Jungclaus *et al.*, Z. Phys. A **340**, 125 (1991).
[7] M. K. Kabadiyski *et al.*, Phys. Rev. C **50**, 110 (1994).
[8] J. A. Sheikh, N. Rowley, M. A. Nagarajan, and H. G. Price, Phys. Rev. Lett. **64**, 376 (1990).
[9] I. Ragnarsson, S. G. Nilsson, and R. K. Sheline, Phys. Rep. 45, 1 (1978).
[10] W. Nazarewicz, J. Dudek, R. Bengtsson, T. Bengtsson, and I. Ragnarsson, Nucl. Phys. **A435**, 397 (1985).
[11] H.-Q. Jin *et al.*, Phys. Rev. Lett. **75**, 1471 (1995).
[12] A. G. Smith *et al.*, Phys. Lett. B **355**, 32 (1995).
[13] C. J. Gross, W. Gelletly, M. A. Bentley, H. G. Price, J. Simpson, K. P. Lieb, D. Rudolph, J. L. Durell, B. J. Varley, and S. Rastikerdar, Phys. Rev. C **44**, R2253 (1991).
[14] S. Mitarai *et al.*, Nucl. Phys. **A557**, 381c (1993).
[15] I. Y. Lee, Nucl. Phys. **A520**, 641c (1990).
[16] D. G. Sarantites, P. -F. Hua, M. Devlin, L. G. Sobotka, J. Elson, J. T. Hood, D.R. LaFosse, J.E. Sarantites, and M.R. Maier, Nucl. Instrum. Methods (to be published).
[17] M. Weiszflog *et al.*, Z. Phys. A **342**, 257 (1992).
[18] M. K. Kabadiyski, K. P. Lieb, and D. Rudolph, Nucl. Phys. **A563**, 301 (1993).
[19] S. Mitarai *et al.*, Z. Phys. A **344**, 405 (1993).
[20] P. Chowdhury *et al.*, Phys. Rev. Lett. **67**, 2950 (1991).
[21] J. Heese *et al.*, Phys. Rev. C **49**, 1896 (1994).
[22] R. Gross and A. Frenkel, Nucl. Phys. **A267**, 85 (1976).
[23] W. D. Luo and Y. S. Chen, Nucl. Phys. **A564**, 413 (1993).
[24] E. Kirchuk, P. Federman, and S. Pittel, Phys. Rev. C **47**, 567 (1993).
[25] S. M. Harris, Phys. Rev. **138**, B509 (1965).
[26] C. J. Gross *et al.*, Nucl. Phys. **A535**, 203 (1991).
[27] D. Rudolph *et al.*, J. Phys. G **17**, L113 (1991).
[28] A. W. Mountford, J. Billowes, W. Gelletly, H. G. Price, and D. D. Warner, Phys. Lett. B **279**, 228 (1992).
[29] M. Weiszflog, J. Billowes, J. Eberth, C. J. Gross, M. K. Kabadiyski, K. P. Lieb, T. Mylaeus, and D. Rudolph, Nucl. Phys. **A584**, 133 (1995).
[30] J. Dudek, W. Nazarewicz, and N. Rowley, Phys. Rev. C **44**, 1489 (1987).
[31] T. Bengtsson and I. Ragnarsson, Nucl. Phys. **A436**, 14 (1985).
[32] A. V. Afanasjev and I. Ragnarsson, Nucl. Phys. **A586**, 377 (1995).
[33] J. Döring *et al.* (unpublished).
[34] I. Ragnarsson *et al.*, Phys. Rev. Lett. **74**, 3935 (1995).
[35] A. V. Afanasjev and I. Ragnarsson, Nucl. Phys. **A591**, 387 (1995).